Short communication

The Effect of Ti Doping on the Electrochemical Performance of Lithium Ferrite

Keqiang Ding[1,], Jing Zhao[1], Mian Zhao[2], Yuying Chen[1], Yongbo Zhao[1], Jinming Zhou[1,*]*

[1] College of Chemistry and Materials Science, Hebei Normal University, Shijiazhuang 050024, P.R. China
[2] Huihua College of Hebei Normal University, Shijiazhuang 050091, P.R. China
[*]E-mail: dkeqiang@263.net, zhoujm@iccas.ac.cn

For the first time, a novel composite anode material of titanium (Ti)-doped lithium ferrite (denoted as Ti/LFT) was successfully prepared under air conditions by a high temperature solid state reaction. In this work, the influence of Ti:Fe atomic ratio on the electrochemical performance of the produced Ti/LFT composite was systematically investigated. The crystal structure and morphology of the prepared Ti/LFT composite material were probed by X-ray diffraction (XRD) and scanning electron microscope (SEM). And the electrochemical performance of the resultant materials was chiefly studied by using cyclic voltammetry (CV), electrochemical impedance spectroscopy (EIS) and galvanostatic charge-discharge tests. Results of the electrochemical tests substantially demonstrated that as the atomic ratio of Ti to Fe was 1:8, the best electrochemical performance was exhibited by the as-prepared composite, showing an initial discharge capacity of 761 $mAhg^{-1}$ at the current density of 100 mAg^{-1} and better rate capability (200 $mAh\ g^{-1}$ at 700 $mA\ g^{-1}$), which was markedly superior to the pure lithium ferrite that was prepared using the same process in the absence of Ti-doping.

1. INTRODUCTION

Iron oxide-based electrode materials for lithium ion batteries (LIBs) have attracted enormous research interest mainly due to their low cost and environmental friendliness [1]. To our knowledge, there are three kinds of iron oxide-based materials, i.e., $LiFeO_2$, $LiFe_5O_8$ and the Fe_2O_4-based material, which have been widely investigated recently. It has been found that $LiFeO_2$ could be employed as a cathode material in LIBs. For example, Morales [2] prepared lithium ferrite by using a simple and

quick method, in which FeOOH, $LiNO_3$ and LiOH were utilized as the starting materials. In his work, when cycled between 4.5V and 1.5V, s-shaped charge/discharge curves were displayed and no voltage plateaus were found. The discharge capacity value at the 9th (C/4) cycle was only 150 mAh g^{-1}, much lower than that of the present commercial cathode material. Although, due to its superior properties such as the high curie temperature, the presence of a hysteresis loop, high saturation magnetization and good thermal stability, lithium ferrites of $LiFe_5O_8$ has been extensively studied in the previous work [3], the research works of using it as electrode materials for LIBs have not been published probably due to its lower theoretical capacity. Among these three kinds of iron oxide-based materials, Fe_2O_4-based electrode materials were the most widely investigated iron oxide-related materials, owing to their high theoretical specific capacity, environment-friendliness [4]. For example, $ZnFe_2O_4/C$ composite microspheres could deliver an enhanced specific reversible capacity of around 1100 mAh g^{-1} at the specific current of 0.05 A g^{-1} after 100 cycles [5]. It was reported that $CoFe_2O_4$ composited with graphene could show a capacity of 325 mAh g^{-1} after 100 cycles at 100 mA g^{-1}[6] and the capacity of $NiFe_2O_4$ could be maintained over 520 mAh g^{-1} after 300 cycles at current density of 1000 mA g^{-1} [7]. It should be noticed that all the reported Fe_2O_4-based materials were prepared in the absence of lithium resources, thus, Fe_2O_4-based material should not be nominated as lithium ferrite. Recent works, also, have revealed that due to their large volume variation during the charge/ discharge process and the poor electrical conductivity, the capacity fade of Fe_2O_4-based electrode material was obvious which greatly hindered their further commercialization in LIBs.

Meanwhile, owing to their excellent reversibility and security capability, some transition metal oxides like iron oxide [8], cobalt oxide [9] and manganese oxide [10] have been paid much more attention for their potential applications in the field of lithium storage. Among these candidate materials, titanium dioxide [11] was regarded as a promising alternative anode material mainly because of its extensive sources, low cost, non-toxicity, high chemical stability as well as the low volume variation during discharge-charge process, though the intrinsic electronic conductivity of TiO_2 was relatively poor which prevented TiO_2 from enhancing practical lithium storage properties in some degree. Although numerous papers concerning iron oxide-based as well as titanium oxide-based electrode materials have been published every year, to the best of our knowledge, till present, no paper reporting the Ti-doped or titanium oxide doped lithium ferrites was published so far.

In this work, Ti-doped lithium ferrites were successfully prepared in air by a high temperature solid state reaction. The influence of atomic ratio of Ti to Fe on the electrochemical performance of the resultant samples was studied. More importantly, the prepared composite exhibited acceptable electrochemical performance when compared to the pure lithium titanate (LTO). Also, the preparation method of this developed composite was rather simple, which is suitable for the large-scale production.

2. EXPERIMENTAL

2.1. Preparation of Ti-doped lithium ferrite (Ti/LFT) composites

Ti-doped lithium ferrite (named as Ti/LFT) composite was fabricated under the air condition by a high temperature solid state reaction method. For instance, the preparation of the sample with the

atomic ratio of Ti to Fe 1:1 was conducted as follows, firstly, 2.180 g of concentrated nitric acid was dissolved in 40 mL distilled water to form a nitric acid solution, and 0.500 g of ferric oxide (Fe_2O_3) was dissolved into above nitric acid solution which was stirred vigorously for 20 min, and then 1.279 g of lithium acetate ($LiAc \cdot 2H_2O$), 0.400 g of glucose, and 3.970 g of oxalic acid were dissolved in above iron-containing nitric acid solution (solution **1**). Meanwhile, 2.19 g of tetrabutyl titanate was dissolved in 30 mL absolute alcohol generating an alcohol solution (solution **2**). Lastly, solution **2** was added into solution **1** drop by drop under vigorous stirring, and the resulting solution was continuously stirred for 1 h, and then the solution was heated in an air dry oven at 150 °C for 3h to produce the precursors. At last, the precursors were thoroughly ground in an agate mortar for about 15 min to form powders, and then, the powders were pressed into pieces by using a tablet compression machine. Finally, the obtained pieces were sintered at 800 °C for about 10 h in a muffle furnace under air conditions to prepare the Ti-doped lithium ferrite (Ti/LFT) composites.

To study the influence of atomic ratio of Ti to Fe, the amount of lithium acetate was kept identical and the atomic ratios of Ti to Fe varied correspondingly to produce the Ti-doped lithium ferrite (Ti/LFT) composites. The samples with the atomic ratios of Ti to Fe 0:1, 1:8, 1:3, 1:1, respectively, were labeled as sample **a**, **b**, **c** and **d**.

2.2. Material characterization

The crystal structures of the prepared samples were characterized by using a Bruker D8 ADVANCE X-ray diffractometer (XRD) equipped with a Cu Kα source (λ= 0.154 nm) at 40 kV and 30 mA. The morphologies of the resultant materials were observed using scanning electron microscopy (SEM, HITACHI, S-570). To detect the presence of functional groups, fourier transform infrared spectrometry (FT-IR) measurements were conducted on a Hitachi FT-IR-8900 spectrometer (Japan). Energy Dispersive X-Ray Spectroscopy (EDS) spectrum analysis was also carried out on a X-ray energy instrument (EDAX, PV-9900, USA) to analyze the composition of the prepared samples.

In the electrochemical measurements, coin-type cells were used, in which lithium metal foil was used as the counter and reference electrode. To produce the working electrodes, the active materials, acetylene black and polyvinylidene fluoride (PVDF), at a weight ratio of 8:1:1, were mixed in an agate mortar for about 10 min, and then several drops of N-methyl-2-pyrrolidine (NMP) were added into above dry mixture generating a slurry. And then, the slurry was pasted onto an aluminum foil and dried at 120 ºC in vacuum oven (ZK-30AB, Longkou City Factory Furnace, China) for about 6 hours. All detailed preparation processes could be referred to our previous work [12].

Two-electrode half cells were installed in a nitrogen-filled glove box (ZKX, Nanjin NanDa Instrument Plant). And the two-electrode half cells contained lithium metal foil as the negative electrode, Celgard 2400 separator and an electrolyte of 1 M $LiClO_4$ in ethylenecarbonate (EC):diethyl carbonate (DEC):dimethyl carbonate (DMC) (2:5:11,vol.). The electrochemical cycle tests were conducted using a CT-3008W-5V20mA-S4 testing system (Shen Zhen Newware Technology Ltd., China) at various current densities between 0 and 3.0 V at room temperature. CV and EIS

measurements were carried out on an electrochemical workstation CHI660E. The EIS analysis was performed at the amplitude of 5 mV with a frequency range from 100 kHz to 0.1 Hz.

3. RESULTS AND DISCUSSION

3.1 Physical characterization of the prepared samples

The XRD patterns of all the resultant samples are presented in Fig. 1. For comparison, the standard XRD patterns of $LiFeO_2$, Li_2TiO_3 and $LiFe_5O_8$ were all plotted in Fig.1. Apparently, the diffraction peaks in all the patterns are relatively sharp, which suggested that all the prepared samples had a relatively higher crystalline nature. For sample **a**, all the main diffraction peaks corresponding to $LiFeO_2$ were exhibited clearly though a weak peak positioned at 35.8º was also observed. It indicated that in the absence of tetrabutyl titanate $LiFeO_2$ was primarily fabricated by this simple preparation method. When Ti source was added, as shown by pattern b (corresponding to sample **b**), besides the reflection peaks of $LiFeO_2$, the diffraction peaks assigned to $LiFe_5O_8$ were also displayed distinctly. In the case of sample **c**, the diffraction peaks belonging to Li_2TiO_3 and $LiFe_5O_8$ were all exhibited clearly. As for sample **d**, the intensities of the diffraction peaks for $LiFe_5O_8$ attenuated, and the diffraction peak of Li_2TiO_3 became higher and sharper. The results of Fig.1 effectively demonstrated that the prepared samples were composites rather than pure compound.
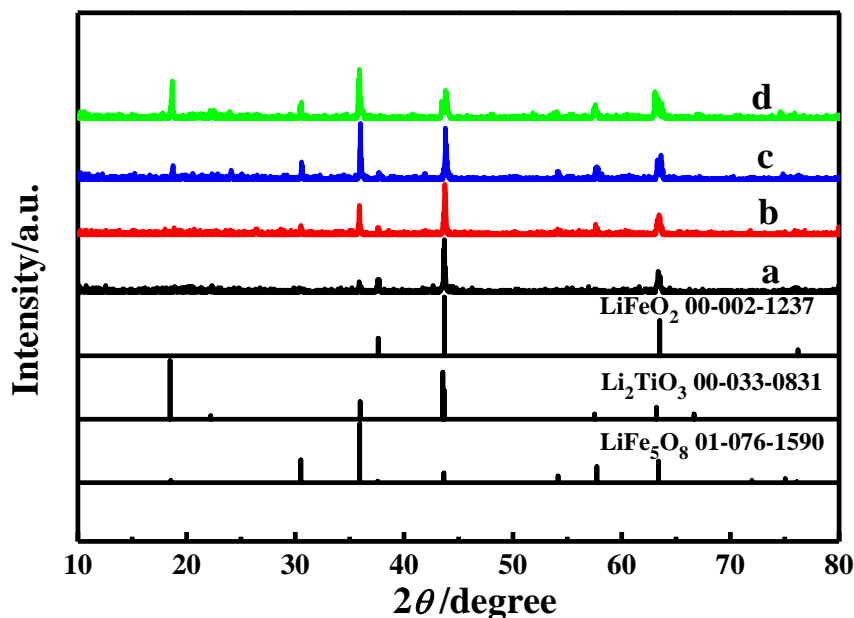
Figure 1. XRD patterns for the resultant samples. Pattern a, b, c and d represented sample **a**, **b**, **c** and **d**.

To further probe the composition of the obtained samples, EDS analysis was conducted and the results are illustrated in Fig.2. For the sample **a**, no element of Ti was detected, which indicated that

LiFeO$_2$ was the main component in sample **a**. For sample **a**, the atomic ratio of Fe to O was 1:1, much larger than the theoretical ratio of 0.5 (Fe to O), which implied that some oxygen-containing impurities were contained in sample **a**. For sample **b**, **c** and **d**, the elements of O, Ti and Fe were all found as presented by curves b, c and d in Fig.2. It should be mentioned that the element of Li cannot be detected by this EDS measurement due to the limitation of the used equipment. The atomic ratios of Ti to Fe in the sample **b**, **c** and **d** were checked to be 0.216, 0.750 and 1.520, respectively. Obviously, the atomic ratios of Ti to Fe in prepared samples were much larger than that of the starting materials, which was probably resulted from the volatilization of the reacting substances during the harsh preparing process.
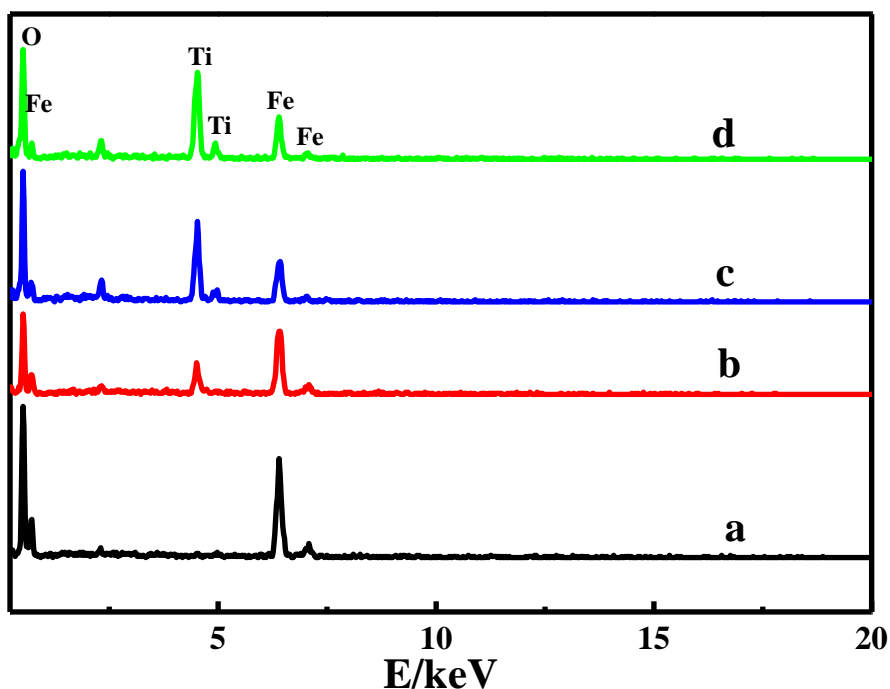
Figure 2. EDS spectra for all produced samples. Spectrum a, b, c and d stood for sample **a**, **b**, **c** and **d**.

To further analyze the composition of the prepared samples, the FT-IR spectra for all the produced samples are given in Fig. 3. Evidently, similar FT-IR spectra were observed for all the samples, which indicated that all the samples had similar functional groups. According to the previous report [13], the bands appearing at about 3462 cm^{-1} should be assigned to the stretching band of OH$^-$. For sample **b** and **c**, the bands at 468 cm^{-1}, 539 cm^{-1} and 602 cm^{-1} are generally ascribed to the stretching vibration modes associated to the metal-oxygen absorption Fe-O bands in the crystalline lattice of prepared material [14]. As for sample **a** and **d**, the bands at 468 cm^{-1} and at 587cm^{-1} were displayed, respectively. Above results documented that although the FT-IR spectra for all the prepared samples were similar to each other, the components of each sample were different from each other.
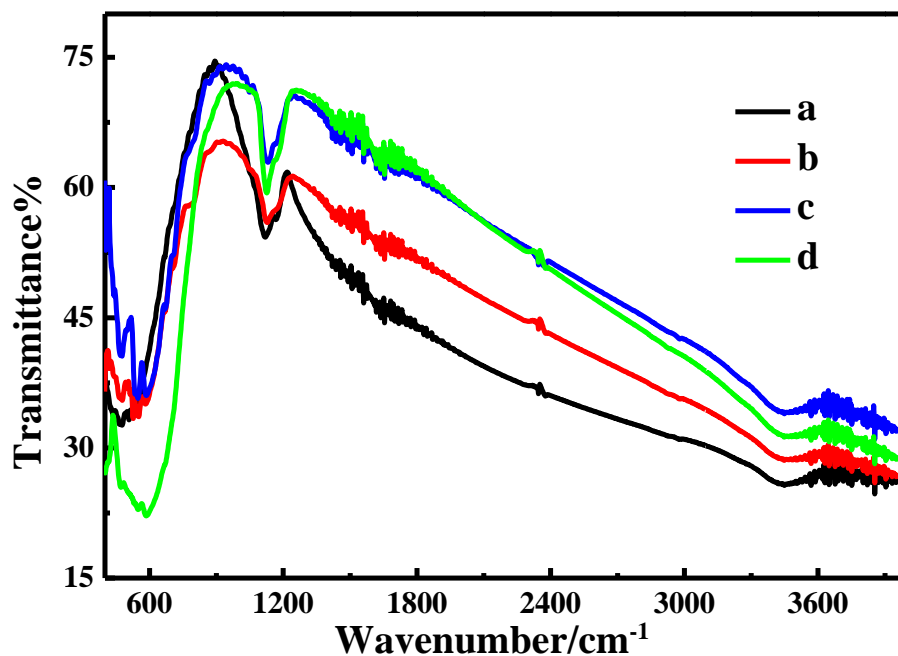
Figure 3. FT-IR spectra obtained for all the samples. Spectrum a, b, c and d represented sample **a**, **b**, **c** and **d**.
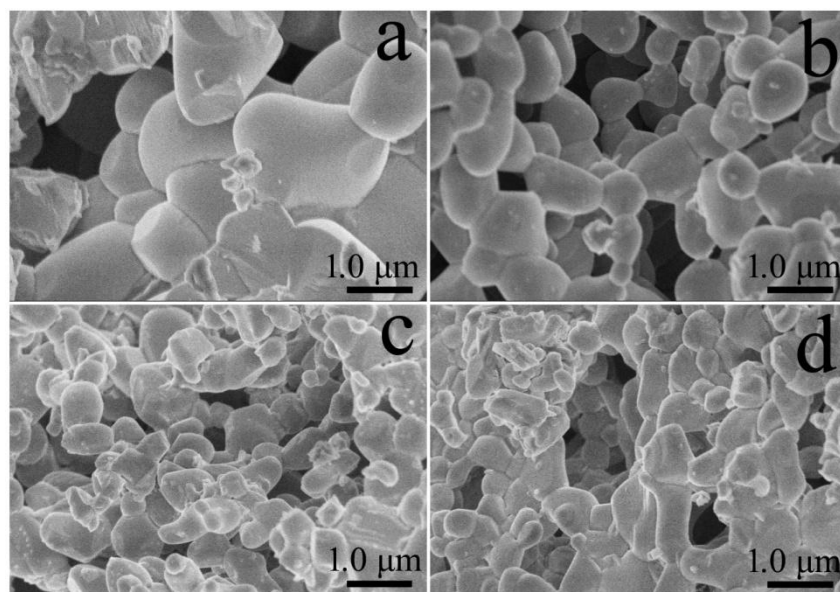
Figure 4. SEM images for the resultant samples. Image a, b, c and d represented sample **a**, **b**, **c** and **d**.

All SEM images for the prepared materials are shown in Fig.4. Apparently, the morphology of each sample was different from each other, which indicated that the composition of each sample was various when compared to other samples. For $LiFeO_2$ (sample **a**), large irregular particles with a size of about 2.4 μm were exhibited. And this particle size was much larger than that of the previously reported $LiFeO_2$ (average size was 40 nm) [15]. While for other samples, much smaller particles were observed. The average particle sizes for sample **b**, **c**, and **d** were, respectively, about 0.90, 0.55 and

0.60 μm. Generally, when the loadings were identical, the smaller particle size would increase the contacting area between the electrode and electrolyte, being favorable for the electrochemical performance of the resultant samples. However, in this case, the compositions of these samples were rather different as verified by the XRD patterns in Fig.1. Therefore, the electrochemical behavior exhibited by the samples should be mainly determined by their components rather than the morphology and particle size displayed. Meanwhile, close observation revealed that the particle size distribution as well as the particle regularity of the sample **b** was superior to sample **c** and **d**. This indicated that the purity of sample **b** outperformed sample **c** and **d**, which may lead to a better electrochemical performance.

3.2. Electrochemical performance

The first (solid line) and second (dashed line) charge/discharge profiles of the four Ti/LFT electrodes at 100 mA g^{-1} are displayed in Fig. 5. For the first charge/discharge profile, the voltage plateaus for the charging and discharging process were centered at 1.46V and 0.64V, respectively. The voltage interval between the charge and discharge voltage plateau was generally related to the polarization loss and the reversibility of a battery cell. The voltage interval for all samples was approximately 80 mV, indicating that the reversibility of all the cells was poor since for a well-defined battery cell the value of voltage interval should be close to zero [16]. The large value of voltage interval was probably originated from the poor electrical conductivity of the prepared samples. Evidently, the initial discharge capacities for sample **a**, **b, c** and **d** were approximately 869,761,710 and 392 mAh g^{-1}, respectively. As for the second charge/discharge curves, the voltage plateaus for all the discharging processes were centered at about 1.04V though the position of voltage plateau for the charging process was not much altered. That is to say, the discharge voltage plateau was increased from 0.64V to 1.04V. The variation of discharge voltage plateau position strongly implied that the inner structures of the samples varied during the charge and discharge process. At the second cycle, the discharge capacities for sample **a**, **b, c** and **d** were approximately 521, 613, 443 and 240 mAh g^{-1}, respectively. Thus, the largest value of discharge capacity was delivered by sample **b**, which was probably due to its large amounts of electrochemical active components. Summarily, this developed material of Ti/LFT has at least two advantages when compared to the spinel lithium titanate ($Li_4Ti_5O_{12}$ (LTO)), first, the discharge capacity for all the prepared samples was markedly higher than the theoretical value of LTO (175 mAh g^{-1}); second, the voltage plateau in the discharging process was 1.04V (vs. Li/Li^+), lower than that of LTO (1.55V vs. Li/Li^+). This meant that a battery with larger capacity and higher output voltage could be produced by using the prepared samples, in comparison with the case of LTO.
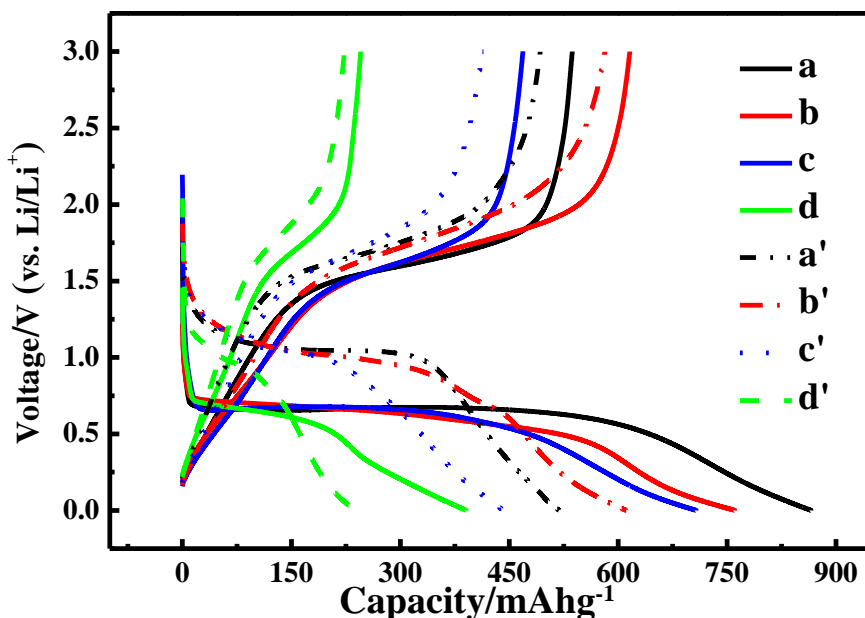
Figure 5. The first (solid line) and second (dashed line) charge-discharge profiles for the prepared cells obtained at 100mA g⁻¹. Curves a and a', b and b', c and c', d and d' were recorded by using sample **a**, **b**, **c** and **d**.

In order to study the cycling performances of the electrodes, the curves of discharge capacity against cycling number were given as shown in Fig.6. The tendency that the discharge capacities slightly decreased with increasing the cycling number was evident. Meanwhile, a large drop of the discharge capacity between the first and second cycle was observed for all the samples, which was reported to be closely related to the formation of solid electrolyte interphase (SEI) layer on the electrode surface [17]. In our opinion, besides the generation of SEI layer, the structure of the electrode materials would be also adjusted especially in the initial charge-discharge process. Or in other words, electrons (in the discharging process) and positive charges (in the charging process) supplied by the charge-discharge instrument would change the structure of the materials used in the battery cell, leading to a novel balance state of the structure. That is to say, it is more rational to use the discharge capacity of the second cycle for evaluating the capacity property of a lithium ions battery. Obviously, sample **b**, except for the first cycle, showed the largest capacity value in the whole testing period. The discharge capacities for sample **a**, **b**, **c** and **d** decreased from 518, 606, 431, 231mAh g⁻¹ at second cycle to 271, 422, 231 and 165 mAh g⁻¹ at the twentieth cycles, respectively. Thus, the capacity retentions for sample **a**, **b**, **c** and **d** were 52.3%, 69.6%, 53.6% and 71.4%, respectively. Hence, sample **b** delivered the highest discharge capacity and maintained the relatively higher capacity retention among all the prepared samples. It should be underlined that the discharge capacities exhibited by sample **a**, **b** and **c** were all significantly higher than the theoretical capacity value of LTO, which was one main contribution of this research work.
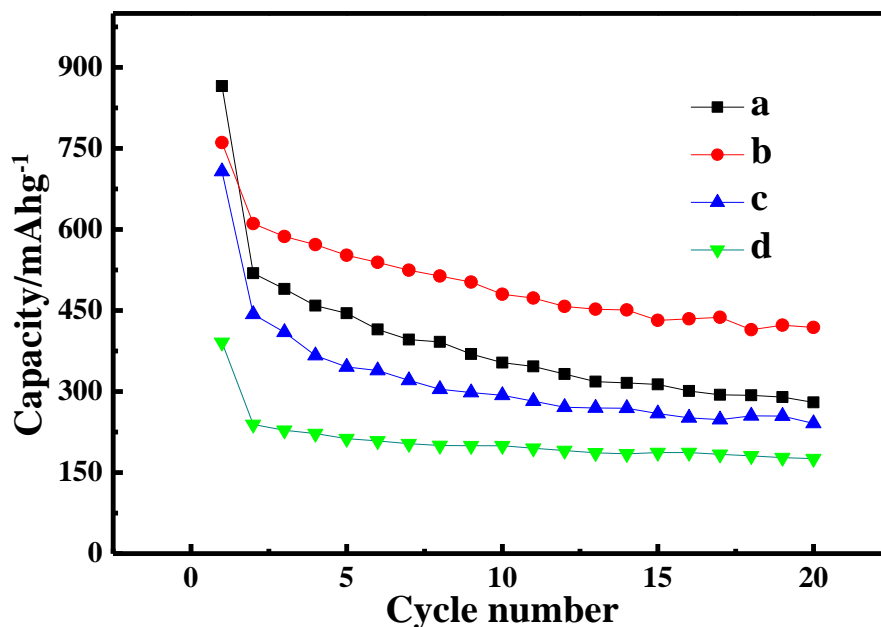
Figure 6. Cycle performance of the prepared various electrodes recorded at 100 mA g^{-1}, line a, b, c and d were plotted by using sample **a**, **b**, **c** and **d**.

Rate capability of an electrode material is a key factor which could effectively affect its practical applications (especially when being quickly charged or discharged). Thus, the rate capabilities of prepared electrodes at different current densities were compared as plotted in Fig.7. It should be noted that for each rate testing, the cell was cycled for 10 cycles.
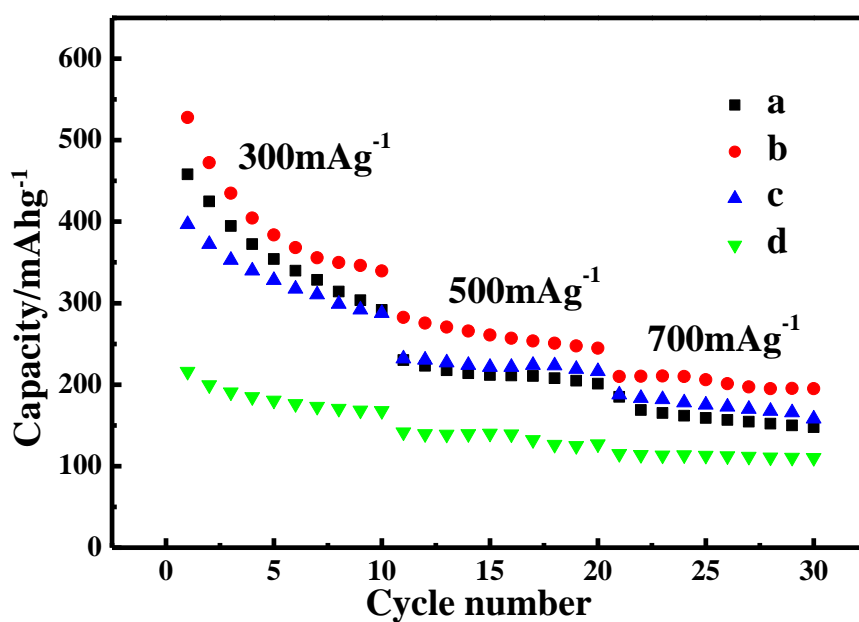
Figure 7. Comparison of the rate capabilities, line a, b, c and d were measured by using sample **a**, **b**, **c** and **d**.

Explicitly, sample **b** showed the largest discharge capacity values at the same rate test among all the samples, and sample **d**, instead, delivered the lowest value of discharge capacity in all rate tests. Meanwhile, it can be seen that at the current density of 300 mA g^{-1}, for sample **a**, **b** and **c**, the discharge capacity dropped rapidly with increasing the cycling number, and at the higher current density of 700 mA g^{-1}, the discharge capacity dropped slightly. This result indicated that the discharge capacity value was not only related to the composition of the electrode material but also to the current density applied. Sample **b** delivered a discharge capacity of around 200 mAh g^{-1} at the current density of 0.7A g^{-1}, which was a comparable value relative to that of LTO. Therefore, the results of Fig.7 testified that the best rate capability was exhibited by sample **b**.

It is well known that electrochemical impedance spectroscopy (EIS) measurement has been widely employed as a powerful technique to examine the charge transfer process occurring in a half cell [18]. Fig.8 shows the typical Nyquist plots, one common curve of EIS plots, for all the half cells assembled by the prepared electrodes. According to the previous report [19], the semi-circle appearing in the high frequency region generally was related to the charge-transfer-limited process that existed at the interface of electrodes, and the inclined line in the lower frequency region was ascribed to the Warburg factor being associated with the diffusion-controlled process of the Li ions in the prepared electrode materials. Commonly, the value of the diameter for the semicircle on the Z' axis approximately was equal to the value of the charge transfer resistance (R_{ct}). Therefore, the values of R_{ct} for sample **a**, **b**, **c** and **d** were roughly estimated to be 175, 52, 200 and 247 Ω, respectively. Generally, the smaller value of R_{ct} was, the faster charge transfer process was achieved. This result effectively proved that the intercalation/deintercalation process of Li ion in the half cell constructed by sample **b** was easier than that in other cells, which was consistent with the results obtained in electrochemical measurements (Fig. 6 and Fig.7).
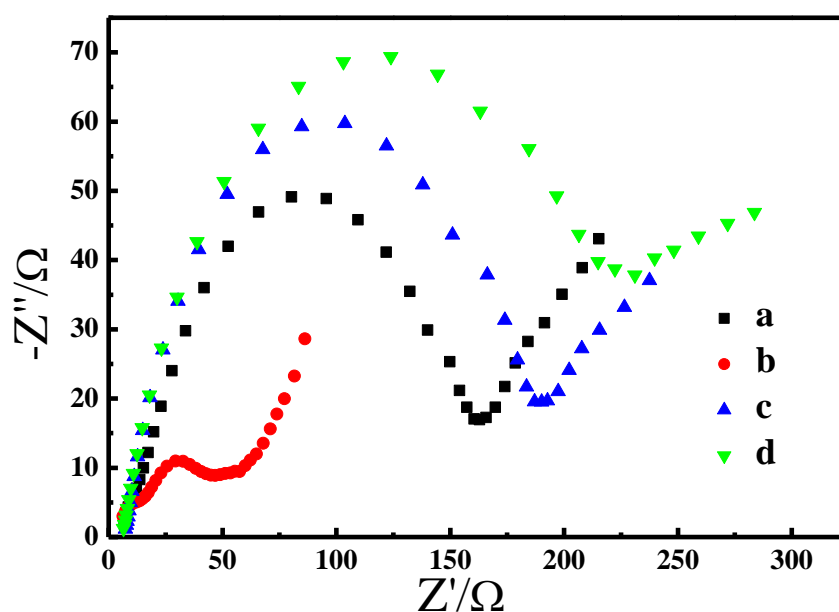
Figure 8. Nyquist plots spectra obtained at the open circuit potentials for all the prepared electrodes in which the frequency range was from 100 kHz to 0.1Hz. Spectra a, b, c and d corresponded to sample **a**, **b**, **c** and **d**.

CV curves of the battery cells constructed by various Ti/LFT electrode materials at a potential scanning rate of 0.5 mV s^{-1} in the potential range from 0V to 3.0 V are displayed in Fig.9. Apparently, well-defined redox peaks were exhibited by these four kinds of cells. Generally, the oxidation peak (positive-direction potential cycling) and the reduction (negative-direction potential cycling) peak stood for the extraction process and insertion process of Li ions, respectively [20]. Thus, this figure indicated that the processes of intercalation and deintercalation for lithium ions could proceed very well in the prepared samples. As expected, sample **d** showed both the lowest oxidation peak current and smallest reduction peak current among all the samples, which happened to account for its poor electrochemical behavior. And, sample **b** showed the highest oxidation peak current as well as the largest reduction peak currents, suggesting that sample **b** had the best electrochemical performance among all the samples. Meanwhile, there were two reduction peaks for all the electrodes. It indicated that the deintercalation process of Li ions proceeded in two stages, which just accorded well with the fact that there were two voltage plateaus in the discharge profiles (Fig.5).
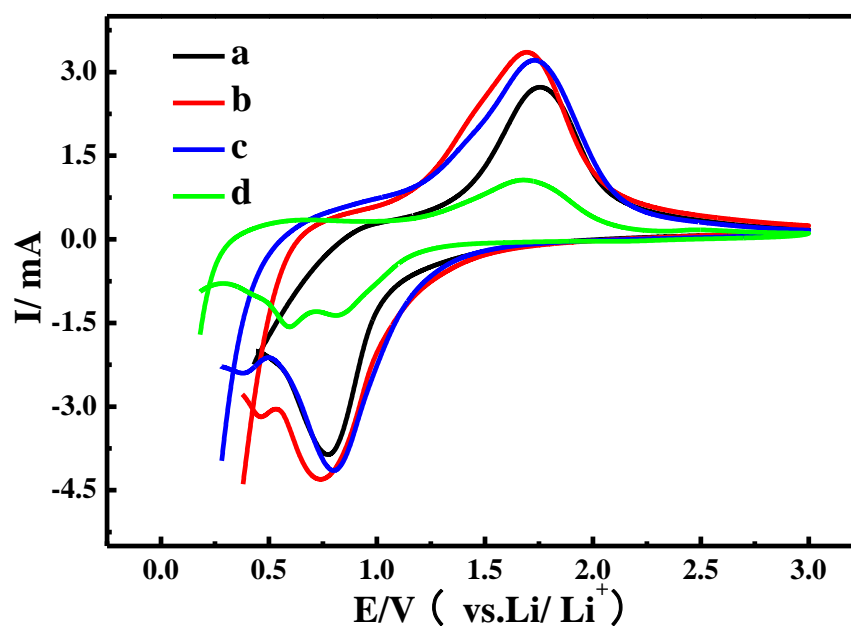
Figure 9. Cyclic voltammograms (CVs) for Ti/LFT electrodes at a scan rate of 0.5 mV s^{-1}. Curve a, b, c and d corresponded to sample **a**, **b**, **c** and **d**.

4. CONCLUSION

For the first time, a novel kind of composite anode material named as titanium (Ti)-doped lithium ferrite (denoted as Ti/LFT) was successfully prepared under air conditions by a high temperature solid state reaction. In the present work, the effect of atomic ratio of Ti to Fe on the electrochemical performance of the produced Ti/LFT composites was systematically probed. In this work, some typical characterization techniques such as XRD, SEM and FT-IR were all utilized. The results of all these characterizations strongly indicated that novel composites were really prepared in

this work. Also, the electrochemical performance of the resultant materials was mainly examined by using CV and EIS measurements. Results from the electrochemical tests demonstrated that as the atomic ratio of Ti to Fe was 1:8, the best electrochemical performance was exhibited, showing higher capacity (761 mAh g^{-1} at 100 mA g^{-1}) and better rate capability (200 mAh g^{-1} at 700 mA g^{-1}). It should be specially emphasized that the electrochemical results of sample **b** were significantly superior to that of LTO in terms of capacity value and rate capability. The work provided in this paper is believed to be very beneficial for the development of novel anode materials for LIBs.

References

1. L. Wang, L. Zhuo, H. Cheng, C. Zhang and F. Zhao *J. Power Sources,* 283 (2015) 289.
2. J. Morales and J. Santos-Peńa. *Electrochem. Commun.*, 9 (2007) 2116.
3. M.M. Costa, R.S.T.M. Sohn, A.A.M. Macêdo, S.E. Mazzetto, M.P.F. Graça, and A.S.B. Sombra, *J. Alloy. Compd.,* 509 (2011) 9466.
4. H. Yue, Q. Wang, Z. Shi, C. Ma, Y. Ding, N. Huo, J. Zhang and S. Yang, *Electrochim. Acta*, 180 (2015) 622.
5. L. Yao, X. Hou, S. Hu, J. Wang, M. Li, C. Su, M. O. Tade, Z. Shao and X. Liu, *J. Power Sources* 258 (2014) 305.
6. L. Wang, L. Zhuo, C. Zhang and F. Zhao. *J. Power Sources,* 275 (2015) 650.
7. N. Wang, H. Xu, L. Chen, X. Gu, J. Yang and Y. Qian, *J. Power Sources,* 247 (2014) 163.
8. Y. Huang, Z. Lin., M. Zheng, T. Wang, J. Yang, F. Yuan, X. Lu, L. Liu and D. Sun , *J. Power Sources,* 307 (2016) 649.
9. A. Jena, N. Munichandraiahb and S.A. Shivashankar, *J. Power Sources,* 277 (2015) 198.
10. X. Jiang, Y. Wang, L. Yang, D. Li, H. Xu and Y. Ding, *J. Power Sources,* 274 (2015) 862.
11. S. S. Tang, G. R. Li, B. H. Liu and Z. P. Li, *Electrochim. Acta*, 125 (2014) 199.
12. K. Ding, W. Li, Q. Wang, S. Wei and Z. Guo, *J. Nanosci. Nanotechnol.*,12 (2012) 3813.
13. K. Ding, Y. Zhao, M. Zhao, Y. Li, J. Zhao, Y. Chen and Q. Wang, *Int. J. Electrochem. Sci.,* 10 (2015) 7917.
14. X.-b. Wang, W.-f. Zhu, X. Wei, Y.-x. Zhang and H.-h. Chen, *Mater. Sci. Eng.*, B 185 (2014) 1.
15. M. Hirayama, H. Tomita, K. Kubota and R. Kanno, *J. Power Sources* 196 (2011) 6809.
16. G.-Q. Zhang, W. Li, H. Yang, Y. Wang, S. B. Rapole, Y. Cao, C. Zheng, K. Ding and Z. Guo, *J. New Mat. Electr. Sys.,* 16 (2013) 25.
17. X. Wu, J. Guo, M. J. McDonald, S. Li, B. Xu and Y. Yang, *Electrochim. Acta*,163 (2015) 93.
18. K. Ding, J. Zhao, J. Zhou, Y. Zhao, Y. Chen, Y. Zhang, B. Wei, L.Wang and X. He, *Int. J. Electrochem. Sci.,* 11 (2016) 446.
19. K. Ding, H. Gu, C. Zheng, L. Liu, L. Liu, X. Yan and Z. Guo, *Electrochim. Acta*, 146 (2014) 585.
20. K. Ding, Y. zhao, L. Liu, Y. Li, L. Liu, L. Wang, X. He and Z. Guo, *Electrochim. Acta,* 176 (2015) 240.